Journal of Applied Surfaces and Interfaces 1 (1-3) (2017) 7-17

Journal homepage: http://revues.imist.ma/?journal=jasi

ISSN: 2550-4800

https://doi.org/10.48442/IMIST.PRSM/jasi-v1i1-3.8601

JASI JOURNAL OF APPLIED SURFACES AND INTERFACES

Structural study and electrochemical behavior of $KPb_{4-x}Cd_x(PO_4)_3$ (0≤x≤2) in capturing mercury (II) at graphite electrode

S. Lahrich [1], B. Manoun [2] and M.A. El Mhammedi [1,]*

[1] Univ. Hassan 1, Laboratoire de Chimie et Modélisation Mathématique, Faculté Polydisciplinaire, 25000 Khouribga, Morocco.
[2] Univ. Hassan 1, Laboratoire Sciences des Matériaux, des Milieux et de la Modélisation, Faculté Polydisciplinaire, 25000 Khouribga, Morocco.

Received 25 April 2017; Revised 30 June 2017; Accepted 10 July 2017.

Abstract : *A novel mercury (II) sensor was developed by modifying carbon paste electrode by anion-deficient apatite. The later was synthesized using solid reaction and characterized with XRD, FTIR, Raman and electrochemical techniques. The refinement results with Rietveld method shows good agreement between the experimental and calculated XRD patterns with satisfactory reliability factors. All experimental variables involved in the differential pulse anodic stripping voltammetric (DPASV) method were optimized to develop a reliable method to measure low concentration of mercury (II). The interference experiments show that Ag (I), Pb (II), Cd (II), Fe (II) and Cu (II) had little or no influence on the Hg (II) signal. Moreover, the prepared electrode revealed good repeatability. The practicability of proposed method for the determination of Hg (II) in fish and seawater samples has shown the satisfactory results.*

Keywords: *Lacunar apatite; Rietveld method; Differential pulse anodic stripping voltammetry; Seawater and fish.*

1. Introduction

Mercury is an extremely toxic element that occurs widely in nature and even considers itself as a contaminant of the environment [1]. Mercury pollution in natural water is recognized as a serious environmental problem and a major threat to human health due to its high toxicity and its accumulative character in the biota. It has become obvious that even very low concentrations of mercury in natural water, can be accumulated by a factor of up to 10^6 in fish and aquatic mammals [2]. Drinking water, fish and fish products are the main routes of incorporation of mercury into the human body [3]. Mercury can only be measured at the ppm level, the concentration of this element in aquatic environments is often below the ppt level and its concentration in fish ranges from 0.5 to 2 $\mu g\ g^{-1}$. Indeed, a preconcentration step is often required [4]. Hence, the determination and monitoring of mercury in natural water and fish are of great importance.

The most common techniques for determination of mercury are cold vapor atomic absorption spectrometry [5,6], inductively coupled plasma atomic emission/or mass spectrometry (ICP-MS) [7,8], spectrofluorimetry [9,10], atomic fluorescence spectrometry [11], X-ray fluorescence spectrometry [12], gas chromatography [13] and microwave-induced plasma atomic emission spectrometry (MIP-AES) [14]. Some sophisticated instrumental techniques are extensively used as standard methods in determining mercury but they still possess some disadvantages, such as high cost of instruments, matrix interference and time consuming. Electrochemical methods have been most commonly employed for detection of mercury in solution such as, anodic-stripping voltammetry [15] and differential pulse anodic stripping voltammetry [16] due to the relatively inexpensive instrumentation and simple operation procedure.

Several solid electrodes, such as gold electrodes [17-19], platinum electrodes [20], silver electrodes [21], graphite electrodes [22], modified carbon paste electrodes [23] and glassy carbon electrode (GCE) [24,25] have been employed. Knowing that Ag (I), Cu (II), Bi (III) and Au (III) ions represent the most critical elements of interference studies within the electrochemistry of Hg (II) ions [26]. In addition, noble electrodes often suffer from the interference effect for mercury [21].

In this paper, an efficient method to detect mercury (II) was reported at carbon paste electrode modified with $KPb_{4-x}Cd_x(PO_4)_3$ (0≤x≤2). The choice of deficient apatite as electrode material is based on the presence of vacant tunnels in the anion sites. In fact, the physicochemical property of these deficient apatites gives them a great adsorption capacity and high catalytic activity. The modifier was characterized by X-ray diffraction (XRD), infrared spectroscopy (FTIR) and Raman spectroscopy (RAMAN). Sufficient sensitivity have been overcome by using 1.0×10^{-1} mol L^{-1} HCl as electrolyte solution. The proposed method was subsequently applied to determine Hg (II) in seawater and fish samples.

* *Corresponding author: E-mail: elmhammedi@yahoo.fr; fax: +212 23485201 (Mly Abderrahim EL MHAMMEDI)*

2. Experimental

2.1. Equipment and reagents

Starting materials used in the synthesis of $KPb_{4-x}Cd_x(PO_4)_3$ ($0 \le x \le 2$) were cadmium nitrate (Sigma Aldrich), ammonium dihydrogenophosphate ($(NH_4)H_2PO_4$-Riedel de Haën, Germany), PbO and K_2CO_3 (from the analytical grade). Carbon paste was supplied from Carbone Lorraine (Lorraine, France; ref 9900). Mercury nitrates and hydrochloric acid were purchased from Sigma–Aldrich (USA).

The obtained products were examined by X-ray diffraction analysis using a D 2-PHASER de BRUKER-AXS (Cu Kα radiation, k = 1.5406 Å). The diffraction patterns were recorded at room temperature in the range 10–100 in steps of 0.02°. Winplotr, Camail, Dhkl and AFPAR software are used for refinement of apatites compounds. Rietveld's profile analysis method was also used for refinement using the FULLPROF program.

Infrared spectra were carried out for characterization of final products obtained using a Perkin-Elmer FTIR 1600 spectrometer. In fact, 1 % of the powder and 99 % KBr were mixed and ground for used in analysis. The spectra were taken in the range from 400 to 4000 cm^{-1}.

The Raman spectra were recorded with an imaging spectrometer (HoloSpec f/1.8i, Kaiser Optical Systems) equipped with a holographic transmission grating and thermoelectrically cooled two-dimensional multichannel CCD detector (Newton, Andor Technology, 1600-400 pixels, -60 °C).

Electrochemical measurements were carried out by using a Metrohm model 797 VA Computrace from Swiss. A voltammetric cell with three electrodes was used. The carbon paste electrode modified with studied lacunar apatite (LAP-CPE) as a working electrode (WE), a platinum electrode as the auxiliary electrode (AE) and an $Ag/AgCl/Cl^-$ (3 mol L^{-1}) as the reference electrode (RE). A pH-meter sensION™, (pH31) with the glass-Ag/AgCl/KCl (3.00 mol L^{-1}) combined electrode, was used for adjusting pH values. A microwave (Samsung, Triple Distribution System) was used for digestion of fish samples.

The electrochemical impedance measurements were carried out using an impedance analyzer potentiostat (model PGZ 100, Eco Chemie B.V, Utrecht, The Netherlands) driven by the electrochemical systems data processing software (VoltaMaster 4 software).

2.2. Preparation and Rietveld analysis of apatite

$KPb_{4-x}Cd_x(PO_4)_3$ (LAP) compounds were synthesized by mixing the reagents $(NH_4)H_2PO_4$, PbO, K_2CO_3 and $Cd(NO_3)_2.4H_2O$ in an agate mortar. The solid state reaction takes place in the following steps: the samples were heated at 400–600 °C, in order to improve the homogeneity of the mixture and were grinded after each treatment until annealing at 700 °C for 14 h. The progress of reaction was controlled by X-ray diffraction.

The program Fullprof integrated with Winplotr software [27] was used to refine the structures with form factors for neutral atoms. The $P6_3/m$ space group and the atomic positions of the $KPb_4(PO_4)_3$ [28] were used as the starting sets in the refinement procedure for the apatites compounds.

In a first step of the refinement, all the structural parameters were fixed to the literature values and lattice parameters were calculated preliminary from Camail, Dhkl and Affpar software. The half width of the diffraction peaks as a function of 2θ was evaluated by the Caglioti equation [29]. Then, numerous parameters were allowed to vary accordingly to the relative weight amount of the observed phases during the successive refinement cycles. Fittings were performed using pseudo-Voigt peak profile functions and a preferred orientation along [001]. During the final step, the atomic parameters including positional, isotropic temperature and occupancy factors were also refined.

The Pb (II) occupancy factors has been made by assuming that the cations are distributed between the two sites (*6h*) and (*4f*) sites, which were imposed to be fully and complementarily occupied. The cadmium cations are preferentially occupied site (*6h*) with stoichiometric value. The occupancy factors of potassium, phosphorus and oxygen were assumed to be constant, in agreement with the stoichiometry of the apatite. It is worth noting that the refinement has been performed in several steps. Thus, the parameters obtained after each step were introduced to achieve the next step. Consequently, all parameters were freed in the last refinement cycles.

2.3. Preparation of LAP-CPE and electrochemical procedure

The apatite modified carbon paste electrodes were prepared by exhaustively hand mixing a known amount of graphite carbon and apatite powder. The mixture was packed in a cavity of electrode (0.1256 cm^2) and a carbon bar was used for the purpose of electrical contact. The electrode surface was cleaned carefully before performing the experiments.

The electrochemical analysis of mercury (II) was performed in 1.0×10^{-1} mol L^{-1} HCl. The differential pulse anodic stripping voltammograms were recorded between -0.1 V and 0.3 V after optimizing the experimental conditions.

The proposed method was applied to determine mercury in seawater. The four samples of seawaters are from El Jadida, Moulay Abdellah, OCP driving and Sidi Abed [30]. The support electrolytes were prepared by addition of 1.0×10^{-1} mol L^{-1} of HCl to fresh seawater without any previous treatment.

Fish sample (Tuna) was purchased from the harbor of El Jadida-Morocco. The caught fish was transferred to the laboratory in a cool box. In order to prevent any possible pollution during sample analysis, fish samples

were dispatched using a stainless steel knife and dried at 80 °C. Then, the samples were crushed, sieved and maintained in a freezer (-4 °C) until analysis. The digestion of fish samples was performed by heating at microwave, which enables a rapid decomposition of samples. A mass of 1.5 g of dried sample was placed in a microwave digestion vessel and 15 mL of H_2O_2 (30 %) as well as 15 mL of HCl (3.0×10^{-1} mol L^{-1}) were added. The microwave power was fixed to 400 W for 30 min. The sample was cooled at room temperature, filtred and diluted to 50 mL, which was used for electrochemical measurement.

3. Results and discussion

3.1. Characterization and refinement studies of synthesis apatite

The series $KPb_{4-x}Cd_x(PO_4)_3$ ($0\leq x\leq 2$) has been synthesized by solid state reaction. It has been controlled by X-ray diffraction, infrared and Raman spectroscopy. Figure 1 shows the XRD patterns (10–100°) of $KPb_{4-x}Cd_x(PO_4)_3$ ($0\leq x\leq 2$). All the observed reflections for the compositions could be indexed in the hexagonal system with space group $P6_3/m$. The X-ray diffraction patterns show the existence of a single phase for apatite.

The position of LAP peak shifted slightly to higher angles by increasing cadmium content in apatite structure $KPb_{4-x}Cd_x(PO_4)_3$ ($0 \leq x \leq 2$). Figure 2 shows hexagonal lattice parameters (*a* and *c*) and unit cell volume (*V*) of LAP powders calcined at 700 °C. The observed decrease in the cell parameters may be due to the substitutions of larger-size Pb (II) ions (1.19 Å) with Cd (II) ions (0.95 Å).

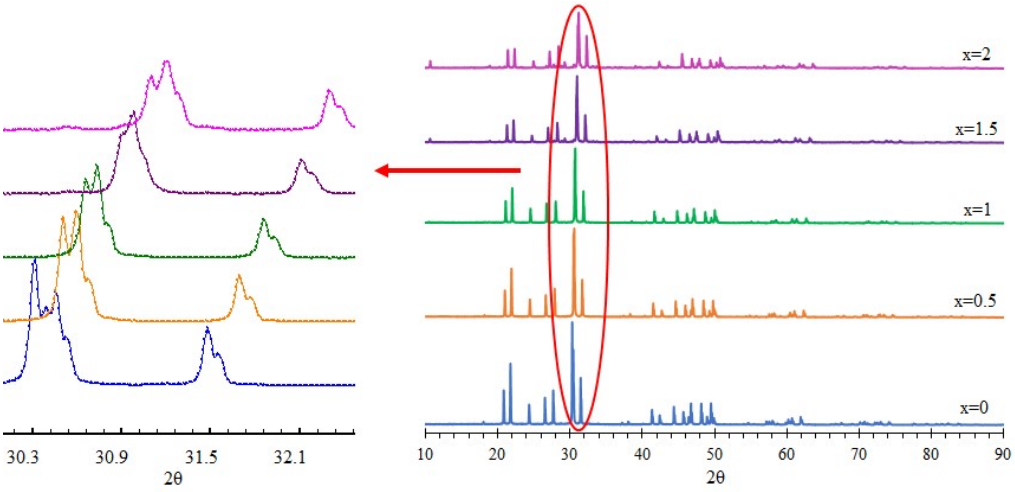

Figure 1. *The X-ray powder diffraction pattern of $KPb_{4-x}Cd_x(PO_4)_3$ ($0 \leq x \leq 2$).*

Figure 3 shows the FTIR spectra of $KPb_{4-x}Cd_x(PO_4)_3$ ($0 \leq x \leq 2$). The characteristic bands of phosphate groups were observed for all the samples. The absorption bands at 600 and 1000 cm^{-1} are characteristic of O-P-O vibration and P-O groups, respectively. The results confirm that these apatites contain the bands characteristic of the phosphate group.

Figure 4 shows the Raman spectra of $KPb_{4-x}Cd_x(PO_4)_3$ ($0 \leq x \leq 2$) recorded at ambient conditions. Raman spectra of all the compositions are similar and show some linear shifts in band positions as a function of the composition toward high frequencies values. This shift is due to the substitution of Pb (II) by Cd (II) with a smaller radius resulting in a decrease of the unit cell parameters. Generally, the observed Raman modes can be classified into three general families of lattice vibrations: K/Pb–O, Pb–O external modes, as well as translational and rotational modes PO_4 tetrahedra, at wave numbers below 350 cm^{-1}; O–P–O bending vibrations, in the 350–700 cm^{-1} region; and P–O stretching modes, at wave numbers over 800 cm^{-1}. However, all of the bands correspond to the stretching and bending vibrations of the P–O bonds in (PO_4) tetrahedra.

Rietveld refinements were carried out using Fullprof program. During the structural analysis, the refined parameters were background coefficients, isotropic thermal parameters, lattice parameters, scale factor, profile half-width parameters (U,V,W), occupancy and atomic functional positions. However, the occupancies parameters did not change. Therefore, following the previously used procedure for apatite Rietveld refinements, the Pb (1), Pb (2) and Cd occupancy were fixed at the stoichiometric values.

For the non substituted sample, the values of *a*= 9.8636 Å and *c*=7.3075 Å are in close agreement with the data reported in the literatures [28]. The decrease of the refined lattice parameters progressively with cadmium content confirms that Cd (II) have entered the apatite structure. The explanation of the lattice contraction can be found in the difference in the sizes of the substituted ions. Indeed, the ionic radius of Pb (II) (1.19 Å) is greater than that of Cd (II) (0.95 Å). The refinement results indicate also a clear preference of Cd (II) ions to occupy site (*6h*) of the apatite structure,

which has been attributed to the ns^2 lone pair electrons of Cd (II).

For the non substituted sample, the values of a= 9.8636 Å and c=7.3075 Å are in close agreement with the data reported in the literatures [28]. The decrease of the refined lattice parameters progressively with cadmium content confirms that Cd (II) have entered the apatite structure. The explanation of the lattice contraction can be found in the difference in the sizes of the substituted ions. Indeed, the ionic radius of Pb (II) (1.19 Å) is greater than that of Cd (II) (0.95 Å). The refinement results indicate also a clear preference of Cd (II) ions to occupy site (6h) of the apatite structure, which has been attributed to the ns^2 lone pair electrons of Cd (II).

The Rietveld refinement data of the prepared lacunar apatite $KPb_{3.5}Cd_{0.5}(PO_4)_3$ as example was shown in Figure 5. The experimental details for the data collection, refinement conditions, the R-factors resulting of Rietveld refinement and also the interatomic bond distances and angles of $KPb_{3.5}Cd_{0.5}(PO_4)_3$ are summarized in Table 1. Hence, the refinement led to a rather good agreement between the experimental and calculated XRD patterns and to satisfied reliability factors. Moreover, the refined structural parameters and atomic positions are presented in Table 2.

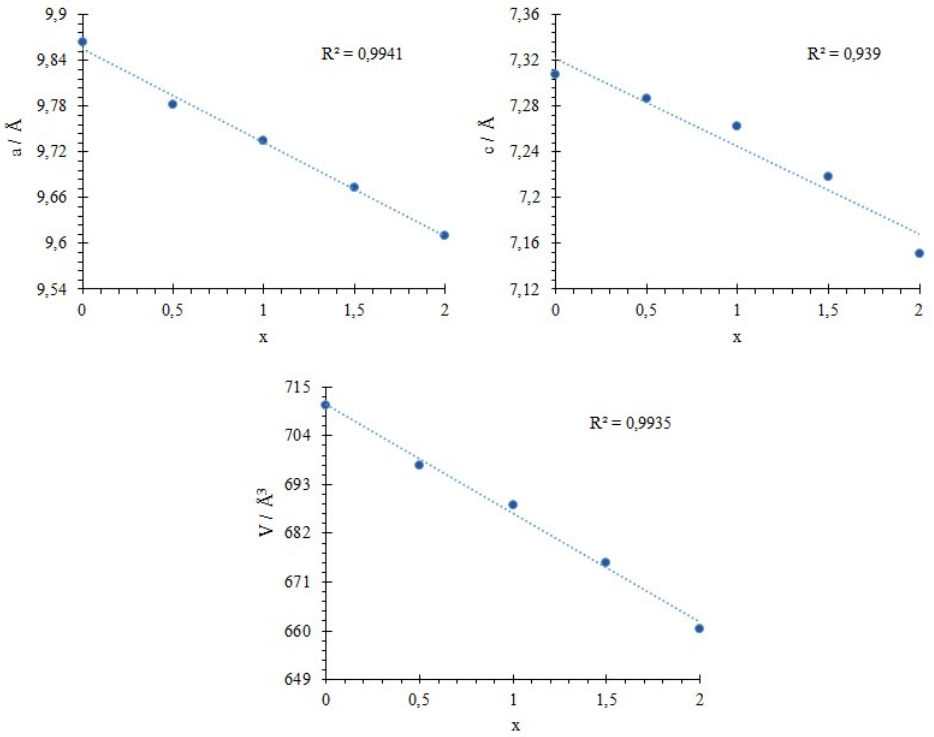

Figure 2. *Unit cell parameter variations as a function of x for $KPb_{4-x}Cd_x(PO_4)_3$ ($0 \le x \le 2$).*

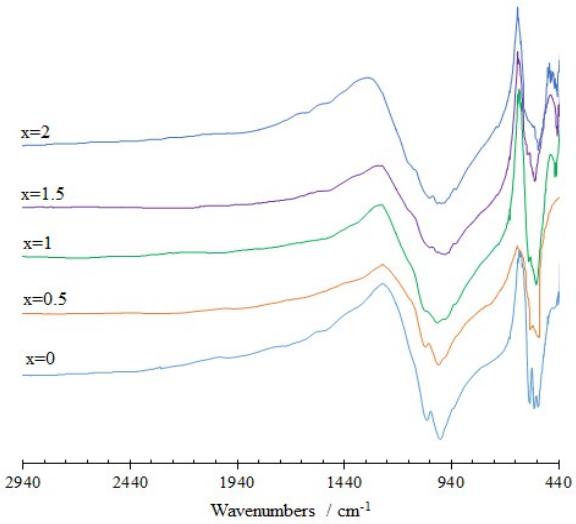

Figure 3. *Infrared spectra of the $KPb_{4-x}Cd_x(PO_4)_3$.*

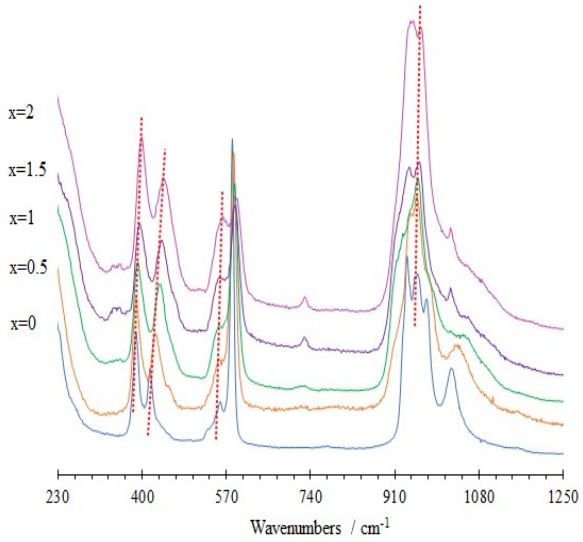

Figure 4. *Raman spectra of the $KPb_{4-x}Cd_x(PO_4)_3$.*

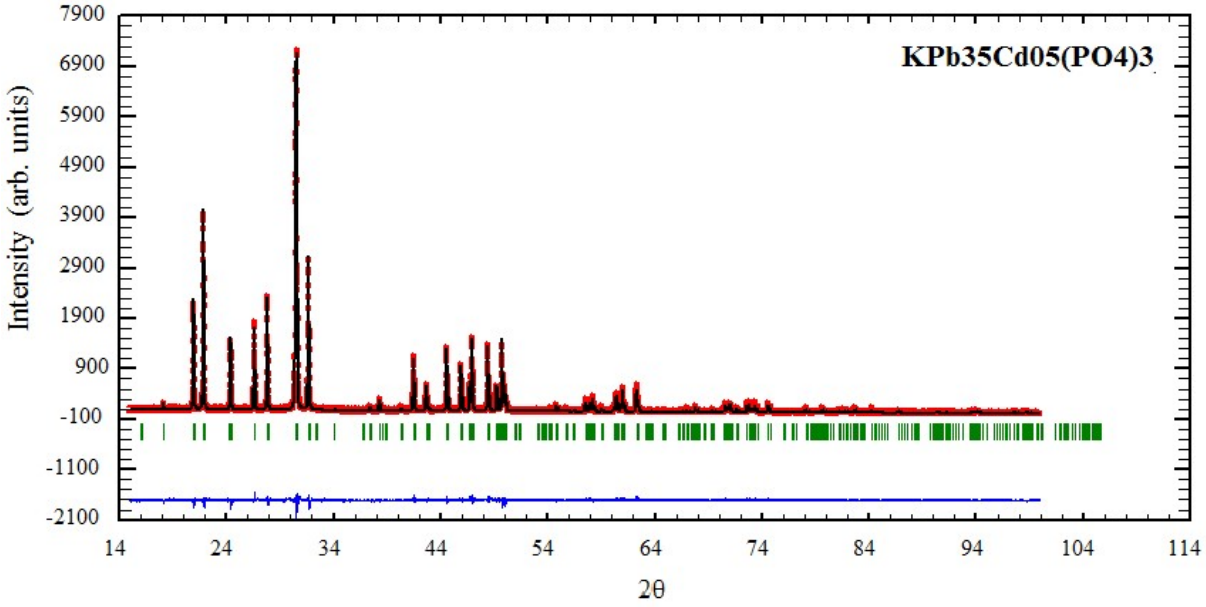

Figure 5. *Final Rietveld plot for $KPb_{3.5}Cd_{0.5}(PO_4)_3$.The upper symbols illustrate the observed data (red circles) and the calculated pattern (black solid line). The vertical markers show calculated positions of Bragg reflections. The lower curve is the difference diagram.*

Table 1

Details of Rietveld refinement conditions and the selected interatomic distances and angles for $KPb_{3.5}Cd_{0.5}(PO_4)_3$.

Composition	x=0.5	Composition	x=0.5
Zero point (°2θ)	0.0359 (4)	Pb / Cd – O (1)	2.81 (2)
Pseudo-Voigt function	0.51635 (17)	2*Pb / Cd – O (2)	2.482 (10)
PV = η L + (1 − η) G		2*Pb / Cd – O (2)	2.696 (15)
Caglioti parameters	0.02430 (128)	Pb / Cd – O (3)	2.263 (16)
	-0.01689 (102)	Pb / K – O (1)	2.447 (15)
	0.00721 (20)	2*Pb / K – O (1)	2.446 (10)
No, of reflections	259	2*Pb / K – O (2)	2.906 (13)
No, of refined parameter	33	Pb / K – O (2)	2.905 (16)
Z	2	2* Pb / K – O (3)	2.691 (12)
Atom number	5	Pb / K – O (3)	2.692 (18)
RF	6.18	P – O (1)	1.63 (3)
RB	4.41	2*P – O (2)	1.577 (12)
Rp	8.0	P – O (3)	1.564 (19)
Rwp	11.5	< P – O>	1.587
cRp	13.7	2* O (1) – P – O (2)	109.7 (18)
cRwp	16.4	O (1) – P – O (3)	110 (2)
Crystal system	Hexagonal	O (2) – P – O (2)	111 (10)
Space group	$P6_3/m$	2* O (2) – P – O (3)	108.1 (12)
		< O – P – O>	109.43

Table 2

Refined structural and atomic position parameters for $KPb_{3.5}Cd_{0.5}(PO_4)_3$.

	x	y	z	B(A²)	Occ
$KPb_{3.5}Cd_{0.5}(PO_4)_3$					
Pb/Cd	0.2559 (3)	0.2591 (2)	0.2500	4.82 (4)	2.5 / 0.5
Pb/K	0.6667	0.3333	0.5067 (10)	4.46 (7)	1 / 1
P	0.3764 (16)	0.4024 (13)	0.7500	5.5 (3)	3
(O1)	0.488 (2)	0.324 (2)	0.7500	7.6 (4)	3
(O2)	0.2711 (16)	0.3484 (15)	0.5708 (15)	7.6 (4)	6
(O3)	0.478 (2)	0.587 (3)	0.7500	7.6 (4)	3

Like all hexagonal deficient apatites, two types of channels can be distinguished in these lacunar apatites [31]. The site (*6h*) is occupied by the lead and cadmium cations with larger section of six-coordination. Whereas, the mixed site is occupied at half by K (I) and Pb (II) cations. These cations coordinated to nine oxygen anions. Indeed, the presence of lone pair ns^2 in hexagonal channels led to stabilization of these lacunar apatites.

3.2. Voltammetric measurement of mercury (II)

Preliminary experiments were carried out to study the general behavior of the Hg (II) at LAP-CPE. Figure 6.A presents differential pulse anodic stripping voltammograms of Hg (II) at unmodified (curve a) and modified carbon paste electrode (curve b) in 1.0×10^{-1} mol L^{-1} HCl (pH 1.37). The increase in anodic current at the modified electrode demonstrates that the lacunar apatite plays an important role in the accumulation process of Hg (II) on the electrode surface.

The effect of cadmium content in lacunar apatites $KPb_{4-x}Cd_x(PO_4)_3$ led to a decrease in current intensity of mercury (II). Thus, the incorporation of Cd (II), especially at high level, into the apatite structure induced led to a certain disorder that may be responsible for the decrease in the apatite stability. Figure 6.B shows that the maximum of anodic current of mercury (II) was obtained with x=0.5 correspond to $KPb_{3.5}Cd_{0.5}(PO_4)_3$. The electrochemical results reveal that the lead (II) plays a crucial role in detecting mercury (II). This property may be due to the presence of lone pairs $6s^2$ [32]. Consequently, stabilizing the apatite structure was performed by the orientation of the lone pairs $6s^2$ of lead within the tunnels. In addition, Pb^{2+} cations with active $6s^2$ lone pair characterized by covalent bond Cd/Pb(1)-O that occupying the hexagonal tunnels. While those located in the mixed sites with an inactive lone pairs $6s^2$ are engaged in an almost ionic bond Cd/Pb(2)/K–O [33]. Knowing that we found difficulties in the analysis using the $KPb_4(PO_4)_3$ (x=0) compound under the same proposed conditions. Indeed, we choose the $KPb_{3.5}Cd_{0.5}(PO_4)_3$ to continuous the study of mercury detection.

3.3. Optimization of the experimental conditions for mercury analysis

In order to quantify mercury, experimental conditions have been optimized using the relationships between peak current (Ip) and physico-chemical parameters. All these parameters exert an intense effect on the peak current.

The influence of the pulse amplitude and the pulse time was studied concurrently on the intensity of anodic current of mercury. The analysis was evaluated in the range of [0.06 V- 0.2 V] and [0.01 s - 0.2 s] for the pulse amplitude and the pulse time respectively. The obtained results demonstrated that an increase in pulse amplitude leads to an increase in scan rate and intensity of current peak, which indicate an adsorption process as the rate-determining step [34]. A significant increase of the signal intensity was observed up to 0.13 V and 0.08 s for pulse amplitude and pulse time respectively.

The effect of the step time and the voltage step was studied simultaneously. The influence of step time was studied in the range from 0.1 to 3.4 s to evaluate the current intensity (Ip) of mercury (II). The current magnitude of the mercury peak was increased with the increase of step time, up to 2 s, longer step time resulted in smaller signals. An increasing of the voltage step from 0.001 to 0.0025 V led to the increase of peak current of Hg (II). However, after 0.0025 V, it caused peak broadening. Therefore, a value of 0.0025 V was chosen as optimal voltage step for further studies.

The effect of the preconcentration time and of the mass of apatite on the responses of Hg (II) were also investigated in the same time. Figure 6.C shows that the anodic peak current of mercury increases with increasing of preconcentration time and the amount of apatite inserted into the cavity of the indicator electrode in parallel. The maximum current intensity was obtained for 45 s and 0.75 % by weight. The anodic peak currents decreased significantly when more than 1 % (LAP, w/w) is used in the electrode preparation. This probably occurs due to the reduction of the conductive area of the electrode surface.

The effect of the deposition potential on the peak current of Hg (II) was studied in the potential range from −400 to 100 mV. The highest efficiency of Hg (II) accumulation onto electrode surface was obtained for a deposition potential of −150 mV. So for further study, the deposition potential of −150 mV was chosen.

The effect of deposition time was also studied for a solution containing 1.0×10^{-5} Hg (II). The results show that the peak current of Hg (II) increases as the deposition time increases and reaches maximum value at a deposition time of 45 s. Hence, the deposition time of 45 s was selected for further work.

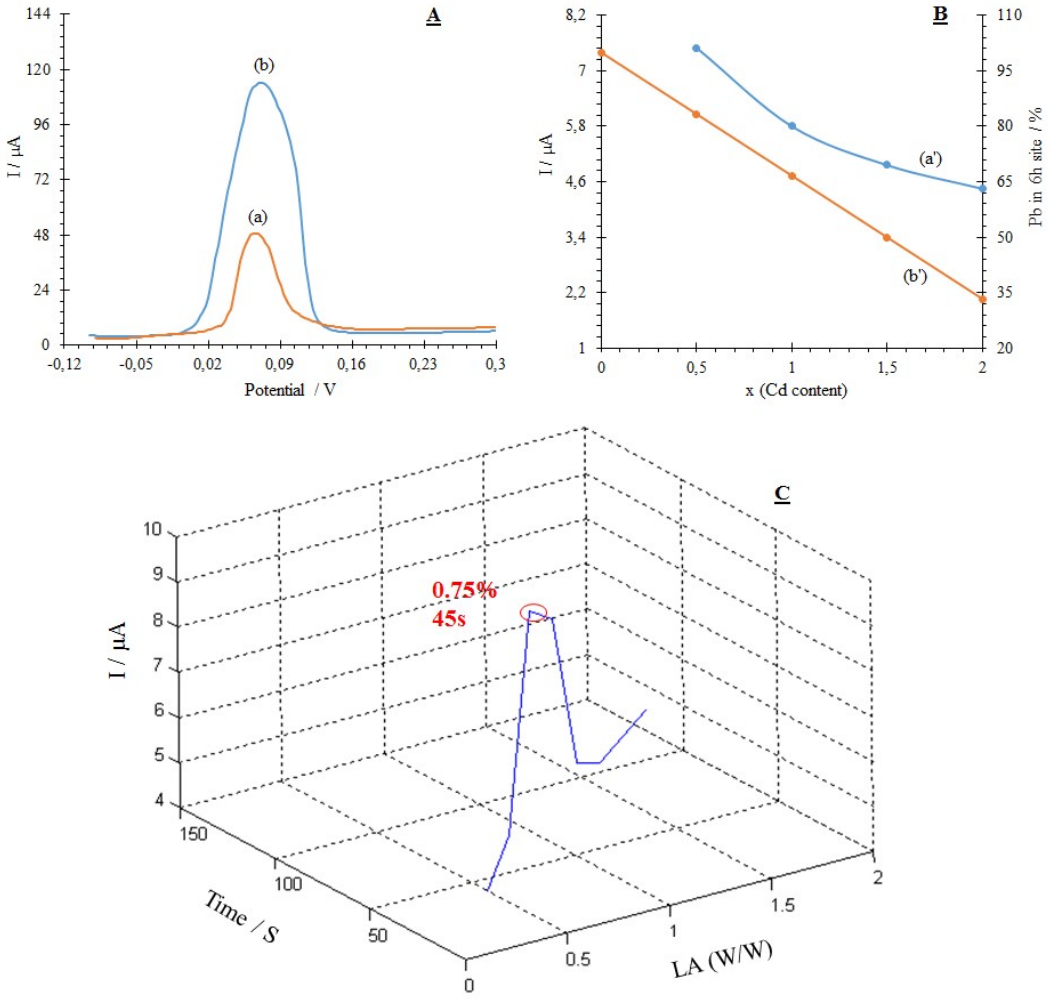

Figure 6 *: **(A)** Differential pulse anodic stripping voltammograms of 1.0×10^{-5} mol L^{-1} mercury (II) in HCl (1.0×10^{-1} mol L^{-1}) at (a) CPE and (b) LAP–CPE (1% LAP). **(B)** Effect of the cadmium content on (a') anodic current intensity of Hg (II) and (b') on the occupancy rate of lead in (6h) site. **(C)** Effect of the preconcentration time and the amount of LAP involved in the DPASV method and response to Hg (II) 1.0×10^{-5} mol L^{-1} in 1.0×10^{-1} mol L^{-1} HCl.*

3.4. Calibration graph, detection limit and interferences effect

Using the optimized parameters, calibration curves were obtained in electrolytic solution containing mercury (II). For this, aliquots from the stock mercury (II) solution were consecutively added to the electrochemical cell. The differential pulse anodic stripping voltammetry responses were recorded in the concentration range from 1.0×10^{-6} to 1.0×10^{-4} mol L^{-1} of mercury (II). The DPASV for different concentrations of mercury (II) were illustrated in Figure 7. The resulting calibration plot and correlation coefficient are (y= 1.1389×10^{-6} [Hg] - 0.5891, R^2=0.9949). The limits of detection (DL,3σ) and quantification (QL,10σ) were 5.36×10^{-7} mol L^{-1} and 1.79×10^{-6} mol L^{-1} respectively. For 9 successive determinations of 7.0×10^{-5} and 1.0×10^{-5} mol L^{-1} Hg (II), the relative standard deviations were obtained as 2.99 % and 6.68 %, respectively. The results demonstrated that the presence of lacunar apatite in the carbon paste could improve both the sensitivity and the repeatability of the modified electrode. The sensitivity is obviously comparable to other electrodes reported in literature (Table 3) [21, 35-40].

In order to evaluate the selectivity of the prepared sensor, the effect of various possible interferents on the determination of Hg (II) was examined. The interferences of electroactive trace elements were studied by addition of these elements to a 5.0×10^{-5} mol L^{-1} mercury solution. The maximum permissible concentrations of interfering metals are shown in Table 4. It was observed that Cd (II), Pb (II), Bi (III), K (I) showed no obvious interference for the determination of mercury (II) and offering the possibility of the simultaneous determination of mercury, bismuth, lead and cadmium. Moreover, it was found that Na (I),

$KMnO_4$ and NH_4 (I) interfered with the determination of 5.0×10^{-5} mol L^{-1} Hg (II) because their presence catalyzes the oxidation of mercury. It is possible to carry out mercury determination in real samples because a large excess of (Na (I), $KMnO_4$ and NH_4 (I)) is rarely found there. By addition of Cu (II), Ag (I) and Fe (II), the mercury peak intensity was increased because of the formation of an amalgam M-Hg. However, the determination was possible if the excess did not surpass a 10 / 1 or 30 / 1 ratio of one of these metals. These interferences can be removed by separating the peaks using the mixture of 1.0×10^{-1} mol L^{-1} HCl, 2.0×10^{-1} mol L^{-1} KNO_3 and 5.0×10^{-1} mol L^{-1} NaCl as supporting electrolyte [21].

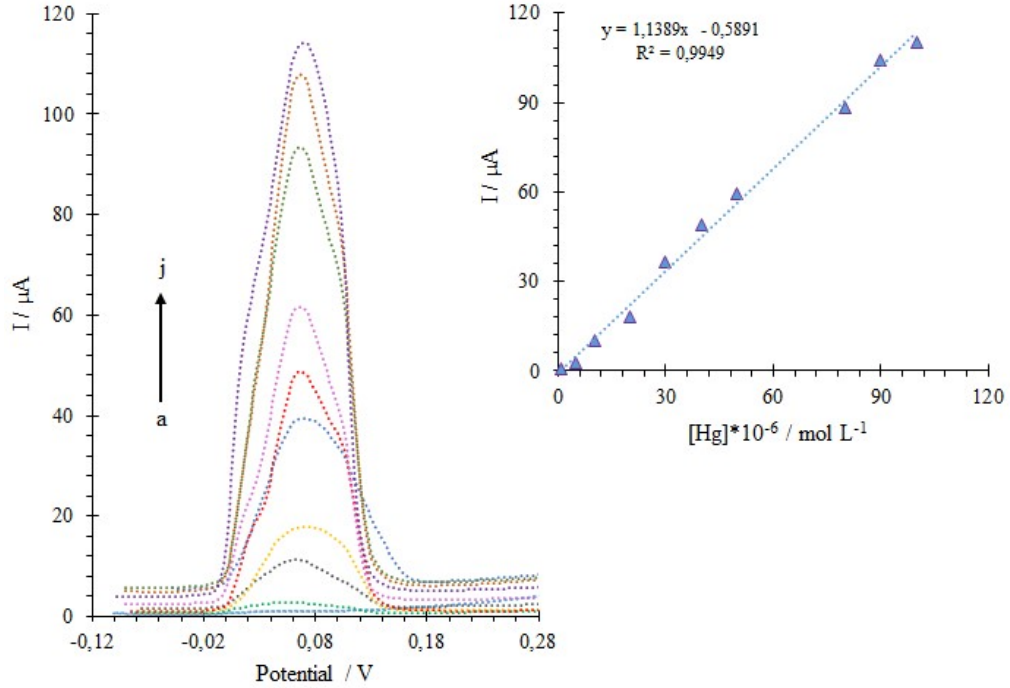

Figure 7. *Calibration curve and respective voltammograms for increasing concentrations of Hg (II) in HCl 1.0×10^{-1} mol L^{-1} under the DPASV optimized conditions at the LAP–CPE. (a) 1.0×10^{-6}; (b) 5.0×10^{-6}; (c) 1.0×10^{-5}; (d) 2.0×10^{-5}; (e) 3.0×10^{-5}; (f) 4.0×10^{-5}; (g) 5.0×10^{-5}; (h) 8.0×10^{-5}; (i) 9.0×10^{-5} and (j) 1.0×10^{-4} mol L^{-1}.*

Table 3

Different electrodes applied for the determination of mercury (II).

Electrodes	Linear range mol L^{-1}	Limit of detection mol L^{-1}	Relative standard deviation (%)	[Refs]
(GUMEAs)	1.0×10^{-8} to 1.0×10^{-6}	1.16×10^{-9}	----	[35]
Silver electrode	1.0×10^{-7} to 8.0×10^{-4}	4.61×10^{-8}	2.19	[21]
MFS–gold electrode	-----	1.0×10^{-7}	----	[36]
N-BDMP–CPE	-----	4.1×10^{-8}	4.7	[37]
P3MT-CE	-----	6.98×10^{-9}	2.5	[38]
BTPSBA–MCPE	2.0×10^{-6} to 10.0×10^{-6}	4.0×10^{-7}	----	[39]
GS-CPE	4.0×10^{-7} to 1.0×10^{-5}	6.5×10^{-8}	3.2	[40]
LAP-CPE	1.0×10^{-6} to 1.0×10^{-4}	5.36×10^{-7}	2.99	Present work

CPE : Carbon paste electrode
GUMEAs : Gold ultra-microelectrode arrays
MFS–gold electrode : Mercaptopropyl functionalized silica / gold electrode
N-BDMP –CPE : Nitro benzoyl diphenymethylenphosphorane modified carbon paste electrode
BTPSBA–MCPE : Carbon paste electrode modified with SBA-15 nanostructured silica organofunctionalised with 2-benzothiazolethiol
GS–CPE : Electrode carbon paste modified by silica gel
P3MT-CE: Carbon electrode modified with poly-3-meth- ylthiophene

3.5. Analytical application in fish and seawater

In order to evaluate the performance of LAP−CPE by practical analytical applications, the determination of mercury (II) was carried out in real samples (seawater and fish). Some tests were carried out for spiked seawater (collected from El Jadida, Moulay Abdellah, OCP driving and Sidi Abed). The standard addition method was used for the determination of mercury (II). The giving relative standard deviations for nine measurements are below 6 % (Table 5). These results indicate that the proposed methodology is suitable for the determination of Hg (II) in seawater samples.

The electrode was also applied to Hg (II) analysis in fish samples. Here, the samples and spiked samples were pretreated by the procedure described in Section 2.4.2. When the method was applied to fish samples, the concentration of the mercury was found to be lower than the limit of detection. The relative standard deviations were performed in appropriate concentrations of mercury. The obtained results, in eight repetitions, for 1.0×10^{-5} mol L^{-1} and 5.0×10^{-5} mol L^{-1} are 6.64 % and 4.19 % respectively. These indicated that the proposed method has a good accuracy and precision.

3.6. Interaction studies of mercury (II) at LAP/CPE electrode

Figure 8-A shows the Nyquist plots of LAP modified electrode interface/solution obtained at abandon potential in 1.0×10^{-1} mol L^{-1} HCl with and without mercury (II) after immersion in the solution for 30 min. These plots are made up of a main form capacitive loop semicircle. This type of graph usually indicates that the interaction between mercury and electrode surface is controlled by a charge transfer process. The charge transfer resistance (Rct) is lower in the case of the presence of mercury than in the case of the control (blank).

Table 4

Maximum permissible concentrations of the interfering metals for the determination of mercury with LAP modified electrodes.

Elements	M: Hg (maximum possible ratio)
Na^+, $KMnO_4$ and NH_4^+	10 / 1
Cu^{2+} and Ag^+	10 / 1
Fe^{2+}	30 / 1
Cd^{2+}, Pb^{2+}, Bi^{3+} and K^+	50 / 1

Table 5

Relative standard deviations for seawater samples in 1.0×10^{-4} mol L^{-1} spiked Hg (II) at LAP-CPE under the optimized conditions.

Hg (II) in Seawaters	
Samples	RSD (%)
El Jadida	5.2
Moulay abdellah	6.13
OCP driving	4.86
Sidi abed	5.09

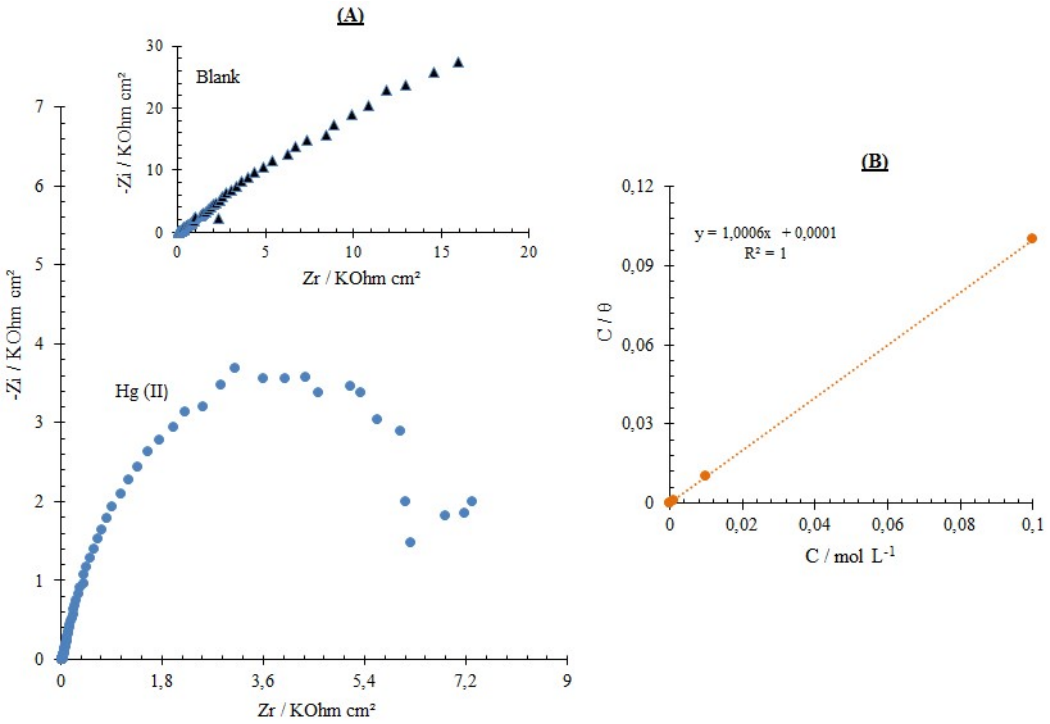

Figure 8. (A) *Impedance spectra in HCl (1.0×10^{-1} mol L^{-1}) with and without mercury (II) after 30 min of insertion.* ***(B)*** *Plot of Langmuir adsorption isotherm of mercury (II) on the LAP/CPE surface.*

The value of Rct, determined from the difference between the low frequency and the high frequency limit of the real part of the total impedance boundary, decreases with the concentration of the mercury (II). Indeed, during the immersion process in electrolytic solution, the mercury was adsorbed on the LAP electrode surface. The layer of mercury thus formed serves as a increasing of electrode conductivity.

The adsorption mechanism of mercury on the LAP/CPE surface was determined by fitting the θ values to Langmuir isotherm at different concentrations according to equation:

$$C/\theta = 1/K_{ads} + C \qquad \text{Eq. 1}$$

where C is mercury concentration, θ is the surface coverage and K_{ads} is the equilibrium constant for the adsorption–desorption process. It was found that the data for the electrode surface coverage θ, corresponding to mercury concentration can be well fitted with Langmuir isotherm where the linear correlation coefficient is R^2=1.

Figure 8-B shows the C/θ in function of C plot of $KPb_{3.5}Cd_{0.5}(PO_4)_3$ deficient apatite. The obtained adsorption coefficient k calculated from the intercept of the plot of Eq 1. The adsorption free energy value ΔG_{ads} can be determined according to Eq. [41]:

$$\Delta G_{ads} = -RT \ln K_{ads} \qquad \text{Eq. 2}$$

where R is the gas constant and T absolute temperature and K_{ads} is the equilibrium constant for the adsorption–desorption process.

The ΔG_{ads} values obtained from k is -32.2 Kj/mol for mercury analysis at LAP/CPE surface. The negative values of ΔG_{ads} ensure the spontaneity of the adsorption process and stability of the adsorbed layer on the metal surface. Generally, value of ΔG_{ads} up to -20 kJ mol^{-1} is ascribed to electrostatic interaction between the charged metal and charged molecules (physisorption), while those around -40 kJ mol^{-1} or higher are associated with chemisorption as a result of a coordinate type of bond between the two [42,43]. Some other researchers have suggested that the range of ΔG_{ads} of chemical adsorption processes in aqueous media lies between -21 and -42 kJ mol^{-1} [44]. The present data is convincing with reference to both of them for chemisorption.

4. Conclusion

$KPb_{4-x}Cd_x(PO_4)_3$ compounds were synthesized with solid state reaction and characterized by XRD, infrared and Raman spectroscopy. Rietveld refinements showed that these solid solutions are continuous adopting $P6_3/m$ space group. Moreover, the electrochemical studies reveal the most interest of lead in lacunar apatite to detecting mercury (II). The influence of the experimental variables, which involved in the DPASV determination of mercury (II), was investigated. The described method has high sensitivity, good linear ranges and low detection limit (5.36×10^{-7} mol L^{-1}) of mercury (II). The analytical advantages of proposed method were presented in the use of 0.75 % by weight of LAP at a very short preconcentration time that does not exceed 45 s. Additionally, the proposed methodology was successfully applied in determining mercury (II) in seawater and fish samples. In perspective, it seems very interesting to test the performance of the proposed method in other kinds of fish that can also accumulate the mercury, such as sardines.

Acknowledgement

The research described in this article has been funded by the university Hassan 1, Morocco.

References

[1] S.C. Foo, T.C. Tan, Sci. Total Environ. 209 (1998) 185–192.
[2] R.P. Mason, F.M.M. Morel, H.F. Hemond, The role of microorganisms in elemental mercury formation in natural waters, in: D. Porcella, J. Huckabee, B. Wheatley (Eds.), Mercury as a global pollutant, Springer Netherlands (1995) 775–787.
[3] H.G. Seiler, A. Sigel, H. Sigel, handbook on metals in clinical and analytical chemistry,CRC Press, New York, 1994.
[4] J.E. Sanchez Uria, A. Sanz-Medel, Talanta 47 (1998) 509–524.
[5] N. Rey-Raap, A. Gallardo, Waste Manag. 32 (2012) 944–948.
[6] Y. Zhang, S.B. Adeloju, Anal. Chim. Acta 721 (2012) 22–27.
[7] H. Shoaee, M. Roshdi, N. Khanlarzadeh, A. Beiraghi, Spectrochim. Acta Part A 98 (2012) 70–75.
[8] A. Giacomino, O. Abollino, M. Malandrino, M. Karthik, V. Murugesan, Microchem. J. 99 (2011) 2–6.
[9] J. Fu, L. Wang, H. Chen, L. Bo, C. Zhou, J. Chen, Spectrochim. Acta Part A 77 (2010) 625–629.
[10] M. Shamsipur, M. Hosseini, K. Alizadeh, N. Alizadeh, A. Yari, C. Caltagirone, V. Lippolis, Anal. Chim. Acta 533 (2005) 17–24.
[11] L. Wu, Z. Long, L. Liu, Q. Zhou, Y.I. Lee, C. Zheng, Talanta 94 (2012) 146–151.
[12] M.L. Carvalho, M. Manso, S. Pessanha, A. Guilherme, F.R. Ferreira, J. Cult. Herit. 10 (2009) 435–438.
[13] Y. Gao, S. De Galan, A. De Brauwere, W. Baeyens, M. Leermakers, Talanta 82 (2010) 1919–1923.
[14] A.M. Carro-Diaz, R.A. Lorenzo-Ferreira, R. Cela-Torrijos, J. Chromatogr. A 683 (1994) 245–252.
[15] E. Bernalte, C.M. Sanchez, E.P. Gil, Anal. Chim. Acta 689 (2011) 60–64.
[16] F. El Aroui, S. Lahrich , A. Farahi, M. Achak, L. El Gaini, B. Manoun, M. Bakasse, A. Bouzidi, M.A. El Mhammedi, J. Taiwan Inst. Chem. Eng. 45(5) (2014) 2725–2732.
[17] Y. Bonfil, M. Brand, E. Kirowa-Eisner, Anal. Chim. Acta 424 (2000) 65–76.
[18] B.K. Jena, C.R. Raj, Anal. Chem. 80 (2008) 4836–4844.
[19] O. Abollino, A. Giacomino, M. Malandrino, S. Marro, E. Mentasti, J. Appl. Electrochem. 39 (2009) 2209–2216.
[20] A. Uhlig, U. Schnakemberg, R. Hintsche, Electroanalysis 9 (1997) 125–129.
[21] A. Farahi, S. Lahrich, M. Achak, M. Bakasse, M.A. El Mhammedi, Sens. Bio-Sensing Res. 4 (2015) 90–95.
[22] S. Perone, W. Kretlow, Anal. Chem. 37 (1965) 968–970.

[23] A. Farahi, M. Achak, L. El Gaini, S. El Yamani, M. Bakasse, M.A. El Mhammedi, Electroanalysis 27 (2015) 1979–1988
[24] M. Hatle, Talanta 34 (1987) 1001–1007.
[25] M. Štulikova, J. Electroanal.l Chem. Interfacial Electrochem. 48 (1973) 33–45.
[26] R. Mikelova, J. Baloun, J. Petrlova, V. Adam, L. Havel, J. Petrek, A. Horna, R. Kizek, Bioelectrochem. 70 (2007) 508–518.
[27] J. Rodriguez-Carvajal, in: Collected Abstracts of Powder Diffraction Meeting, Toulouse, France (1990) 127.
[28] M. Azrour, M. Azdouz, B. Manoun, R. Essehli, S. Benmokhtar, L. Bih, L. El Ammari, A. Ezzahi, A. Ider, A. Ait Hou, J. Phys. Chem. Solids 72 (2011) 1199–1205.
[29] G. Caglioti, A. Paoletti, F.P. Ricci, Nucl. Instrum. 3 (1958) 223–228.
[30] S. Lahrich, B. Manoun, M.A. El Mhammedi, Mater. Res. Bull. 59 (2014) 349 –357.
[31] S. Lahrich, M.A. El Mhammedi, B. Manoun, Y. Tamraoui, F. Mirinioui, M. Azrour, P. Lazor, Spectrochim. Acta A Mol. Biomol. Spectrosc. 145 (2015) 493–499.
[32] R. Ternane, M. Férid, N. Kbir-Ariguib, M. Trabelsi-Ayedi, J. Alloys Compd 308 (2000) 83–86.
[33] M. El Koumiri, S. Oishi, S. Sato, L. El Ammari, B. Elouadi, Mater. Res. Bull. 35 (2000) 503–513.
[34] M. Lovric, S. Komorsky-Lovric, J. Electroanal. Chem. 248 (1988) 239–253.
[35] O. Ordeig, C.E. Banks, J. Del Campo, F.X. Munoz, R.G. Compton, Electroanalysis 18 (2006) 573–578.
[36] A. Walcarius, C. Delacote. Anal. Chim. Acta 547 (2005) 3–13.
[37] A. Afkhami, T. Madrakian, S.J. Sabounchei, M. Rezaei, S. Samiee, M. Pourshahbaz, Sens. Actuators, B 161 (2012) 542–548.
[38] H. Zejli, P. Sharrock, J.L.H.-H. de Cisneros, I.N. Rodriguez, K.R. Temsamani, Talanta 68 (2005) 79–85.
[39] I. Cesarino, G. Marinoa, J.R. Matos, É.T.G. Cavalheiro, Talanta 75 (1) (2008) 15– 21.
[40] L.M. Aleixo, M. de F'atima, B. Souza, O.E.S. Godinho, G. de Oliveira Neto, Y. Gushikem, Anal. Chim. Acta 271 (1) (1993) 143–148.
[41] A.J. Bard, L.R. Faulkner, Electrochemical methods, Wiley, New York (1980).
[42] S.A. Umoren, E.E. Ebenso, Mater. Chem. Phys. 106 (2007) 387–393.
[43] S.A. Umoren, B. Obot, E.E. Ebenso, E-J. Chem. 5 (2008) 355–364.
[44] L. Mali, C. Srivastava, K. Agrwal, M. Mishra, Colloids Surf, A 264 (2005) 17–28.